

https://dspace.org/

Orifice Jet Curvature and Its Interaction With a Row of Short PinFins

Sjouke Schekman; Tong Kim

https://hdl.handle.net/10539/40592
WOS

Downloaded from a DSpace repository. https://dspace.org/

Check for updates

ASME Journal of Fluids Engineering
Online journal at:
https://asmedigitalcollection.asme.org/fluidsengineering

Downloaded from http://asmedigitalcollection.asme.org/fluidsengineering/article-pdf/doi/10.1115/1.4064008/7230895/fe_146_05_051302.pdf by The Nanjing University Of Aeronautics & Astronautics user on 18 January 2024

Orifice Jet Curvature and Its Interaction With a Row of Short Pin-Fins

Sjouke Schekman[1]
School of Mechanical, Industrial, and Aeronautical Engineering, University of the Witwatersrand, Johannesburg 2000, South Africa
e-mail: sjouke.schekman@wits.ac.za

Tongbuem Kim
School of Mechanical, Industrial, and Aeronautical Engineering, University of the Witwatersrand, Johannesburg 2000, South Africa;
College of Aerospace Engineering, Nanjing University of Aeronautics and Astronautics, Nanjing 210016, China

The fluidic behaviors and interactions present in a setup utilizing perforated blockages and downstream pin-fin are elucidated: specifically, the role of jet curvature in flow interactions and the interaction of end-wall flows around the pin-fins subjected to impinging jet. To this end, a combination of particle image velocimetry-based measurements and oil-dye surface flow visualization technique is utilized. Two different configurations of jet flows, with or without flanking jets, and three different distances between the pin-fins and blockages were considered. Jet curvature can result in flow inclinations of as much as 45 deg–60 deg interacting with the pin-fins and the majority of the jet flow is skewed toward the inner side of the pin-fin. At the end-wall, the interaction with nearby structures, being blockages or pin-fins, alters the shape and profile of the flows. This alteration is in contrast to those around conventional pin-fin arrays which remain largely unaltered in the presence of nearby pin-fins. [DOI: 10.1115/1.4064008]

Keywords: pin-fins, perforated blockages, jet impingement, jet curvature, end-wall flows, orifice jets

1 Introduction

Pin-fin arrays and perforated blockages are commonly implemented in engineering applications for cooling purposes. A specific application considered here is the trailing edge of gas turbine blades as shown in Fig. 1. The flow channel is characterized by a narrow height (H) through which coolant flows. Converging end-walls are applicable but for simplicity will not be considered here. In a conventional pin-fin array as shown in Fig. 1(*a*), short aspect ratio cylinders are exposed to a uniform-like flow field. When this flow interacts with the pin-fins it promotes the formation of horseshoe vortices at the base. These flow structures result in an increase of the end-wall heat transfer around the pin-fins. Alternatively, perforated blockages, as shown in Fig. 1(*b*), consist of perforations in the turbine blade internal structures (or "blockages") through which the coolant flow interacts and is forced to pass through. This creates concentrated orifice-like jet flows due to the short thickness-to-diameter ratio ($t/D_j < 2.0$). The jets are targeted at downstream surfaces which are conventionally another perforated blockage in the case of turbine blade trailing edges (Fig. 1(*b*)). But, such surfaces can be those of pin-fins as shown in Fig. 1(*c*) and as depicted in Ref. [1]. In principle, this latter setup (a "blockage pin-fin" setup) focuses the coolant onto the pin-fins for a superior pin-fin array heat transfer.

The cooling performance for internal cooling of turbine blades considers both the heat transfer and friction factor. A blockage pin-fin configuration has, however, received very limited attention due to a poor cooling performance measured in prior studies [2,3]. Specifically, the cooling performance was worse than an empty channel—the internal pin-fins and blockage structures had a detrimental effect. More specifically, the inclusion of perforated blockages increases the friction factor by a factor of ∼100. This purported performance may, however, not be representative for this particular setup. Of specific interest here, as a part of assessing this, is the understanding of the interaction of the orifice-like jet flows with the pin-fins and the resulting end-wall flows.

For a conventional pin-fin array, uniform-like flow convects through the channel, toward the pin-fins. Upon encountering the adverse pressure gradient from pin-fins, the boundary layer separates from the end-wall, rolling up to form a series of vortices upstream of the pin-fins [4]. These vortices wrap around and follow the profile of the pin-fins forming a horseshoe-like pattern as seen in Fig. 2(*a*). Conversely, for a pin-fin subjected to jet impingement, a unique flow field is formed as previousfly revealed by Schekman et al. [5]. The oncoming flow is forced into a jet flow, away from the end-wall, precluding the possibility of an end-wall boundary layer flow upstream of the pin-fin. Horseshoe vortices, therefore, cannot exist and instead, a flow field as shown in Fig. 2(*b*) exists. The jet flow impinges on the pin-fin and is redirected away from the stagnation point on the pin-fin leading-edge surface. A portion of this redirected flow moves toward the end-wall, which subsequently stagnates on the end-wall surface and radiates outwards away from it. The end-wall flow topology is characterized by flows that radiate outwards perpendicularly or tangentially from the pin-fin surface. This is in contrast to the conformal flow patterns of horseshoe vortex structures.

For a row of multiple pin-fins subject to a uniform-like flow, the horseshoe vortex structures remain largely unaltered. This is illustrated in per Fig. 2(*c*) based on measurements in previous studies [6,7]. Typical spanwise spacings (S_{z1}/D as per Fig. 1(*a*)) employed in studies using pin-fin arrays are of the order of ∼2.5. With such spacings, the conformal horseshoe vortex streamlines

[1]Corresponding author.

Contributed by the Fluids Engineering Division of ASME for publication in the Journal of Fluids Engineering. Manuscript received July 14, 2023; final manuscript received October 27, 2023; published online January 17, 2024. Assoc. Editor: Luigi P. M. Colombo.

 Copyright © 2024 by ASME

from neighboring pin-fins do not present end-wall flow with opposing or intersecting vectors. This, however, may not apply for a row of multiple pin-fins subject to jet impingement. The end-wall flows from neighboring pin-fins have opposing vectors as marked in Fig. 2(*d*). The nature of the interaction of these opposing streamlines is unclear. Kan et al. [2] visualized through numerical simulation the flow topology near the end-wall for an array of pin-fins subject to jet impingement. The jets were not geometrically aligned with the pin-fins and the jet flows exhibited curvature in the spanwise (z) direction (parallel to the end-wall surface). These factors contributed to a nonuniform and irregular end-wall flow topology. Consequently, a clear interaction of the end-wall flows cannot be clearly inferred. Further interactions at the end-wall may occur with the upstream perforated blockage. There may also be asymmetrical patterns around the outermost pin-fins in a row. Further, depending on the nature of the end-wall flows interactions, the use of a staggered pin-fin array (the pin-fins being offset in subsequent rows) may not be appropriate for a blockage pin-fin setup. Staggered pin-fins result in superior cooling performance for a conventional pin-fin array [7]. The end-wall flow interactions represent the first area of incomplete understanding that this study seeks to elucidate.

Further, as revealed by Schekman et al. [5], the end-wall flow structures around a pin-fin subjected to jet impingement are solely to those jet flows interacting with the pin-fin in the midheight plane. Changes to the flow distribution and direction prior to impingement can then be expected to alter the end-wall flows. The presence of jet curvature in prior studies [2,3] is, therefore, of importance. Here, "curvature" is taken as the deviation of a jets' trajectory from its original x-axis (illustrated in Fig. 3(*a*)). Jet flows have been previously shown to exhibit curvature without downstream pin-fins or obstacles being present in the flow [8–13]. The curvature is due to the asymmetric presence of neighboring jets. Conventionally, a fully turbulent jet ($\mathrm{Re}_j > 3000$), upon exit, immediately begins to entrain the surrounding fluid toward it [14,15]. The surrounding fluid is both the stationary fluid surrounding the jet and nearby jet flows—the jet entrains the neighboring jets toward itself and vice versa [8–13]. This can cause the jets to curve toward each other (Fig. 3(*b*)). If there is some sort of restoring action a jet's curvature may be prevented altogether. An example is a jet being entrained symmetrically in both directions per Fig. 3(*c*). Besides blockage pin-fin setups, studies of perforated blockages (without downstream pin-fins) [16–20] do demonstrate a very small amount of asymmetric end-wall heat transfer. This may indicate that there exists a small flow curvature—although the actual flow curvature was not directly observed in any of those studies. In those latter cases, the flow curvature would be very small and far less than noted in the results of [2,3].

The curvature in Ref. [2] resulted in an inclined and off-axis interaction of the jet with the downstream pin-fin as illustrated in Fig. 3(*a*). Such interactions serve to shift and distort the heat transfer on the surface of the pin-fin but the overall surface heat transfer is largely similar [21,22]. Although, large inclinations (~45 deg) do result in a slight decrease in the pin-fin surface heat transfer. For the blockage pin-fin configuration, the local end-wall heat transfer around pin-fins subjected to off-axis impingement, however, decreased by approximately half [2,3]. The potential of jets to exhibit flow curvature can then be seen as having a negative effect. This is of notable importance for applications utilizing such setups, such as blockage pin-fin setups. The end-wall flows around pin-fins exposed to jet impingement still require elucidation, as previously discussed. An extension of this is the effect of the jet curvature on the end-wall flows. Further, it is uncertain if any of the prior observed flow curvature in Refs. [2,3] was from the natural behavior of the orifice jets solely (regardless of downstream pin-fins) or if the curvature was exacerbated or manipulated due to factors such as geometric misalignment of the jets and pin-fins used in the setups of those prior setups.

A blockage pin-fin cooling setup has been discounted due to a purported poor cooling performance. It is, however, believed that the cooling performance has been misrepresented due to gaps in the fluidic mechanisms that are featured. The elucidation of these misunderstandings may determine what is necessary in a blockage pin-fin setup to ensure an optimal performance. One misunderstanding was the fluidic behavior of a single pin-fin subjected to jet impingement. This has since been eludicated [5] indicating that superior end-wall heat transfer occurs for smaller blockage to pin-fin distances. There are, however, two further key fluidic behaviors in a blockage pin-fin setup that are recognized to require elucidation. Firstly, the effect of jet curvature on end-wall flows for a pin-fin subjected to jet impingement and how the pin-fins manipulate the jet curvature. Any curvature is taken as being detrimental to the cooling performance. Secondly, the behavior of flow interactions between the end-wall flows around a row of pin-fins exposed to impinging orifice jets formed by perforated blockage. To this end, a series of end-wall flow visualizations and particle image velocimetry (PIV)

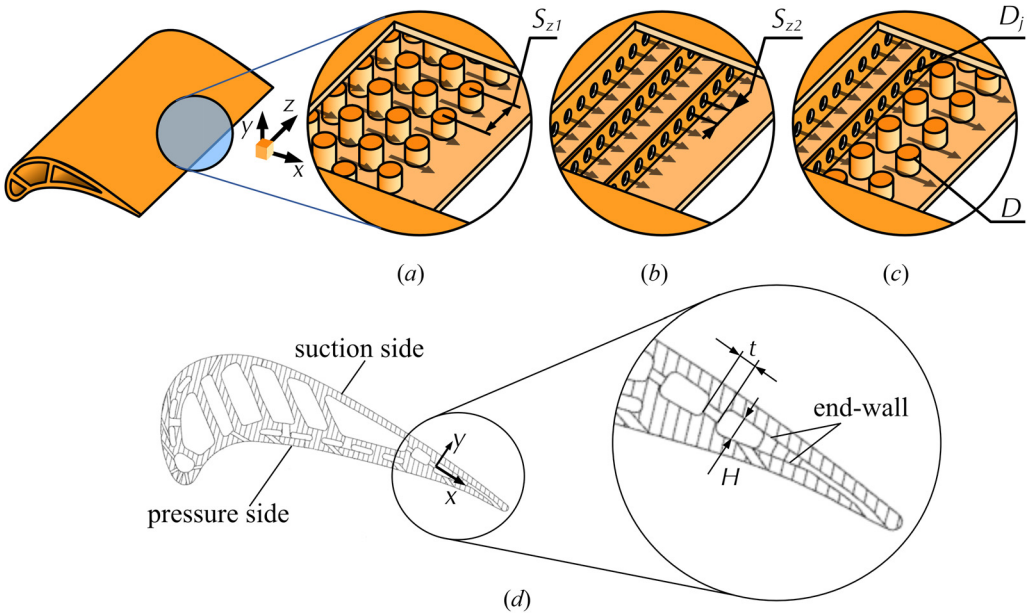


Fig. 1 Turbine blade internal cooling setups at the trailing-edge: (*a*) a pin-fin array, (*b*) perforated blockage plates, (*c*) a combination of perforated blockage and pin-fin array, and (*d*) a cross section of a turbine blade adapted from Ref. [1]

Downloaded from http://asmedigitalcollection.asme.org/fluidsengineering/article-pdf/doi/10.1115/1.4064008/7230895/fe_146_05_051302.pdf by The Nanjing University Of Aeronautics & Astronautics user on 18 January 2024

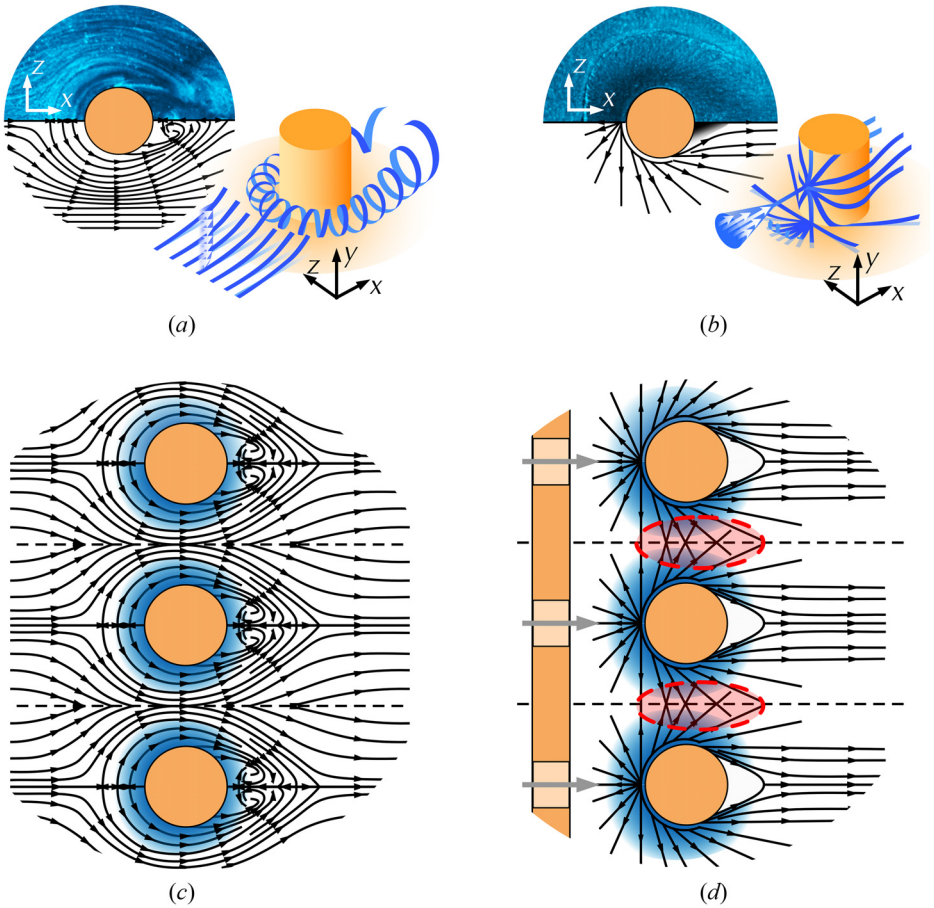


Fig. 2 End-wall flow topologies around short circular pin-fins: (*a*) oil-dye visualization of flow patterns (top) and corresponding flow topology (bottom) with three-dimensional schematic for uniform flow field interaction, (*b*) oil-dye visualization of flow patterns (top) and corresponding flow topology (bottom) with three-dimensional schematic for jet impingement, (*c*) flow patterns for multiple pin-fins with uniform flow field interaction, and (*d*) proposed flow patterns for multiple pin-fins with jet impingement with interaction region between pin-fins marked by the dashed ellipses

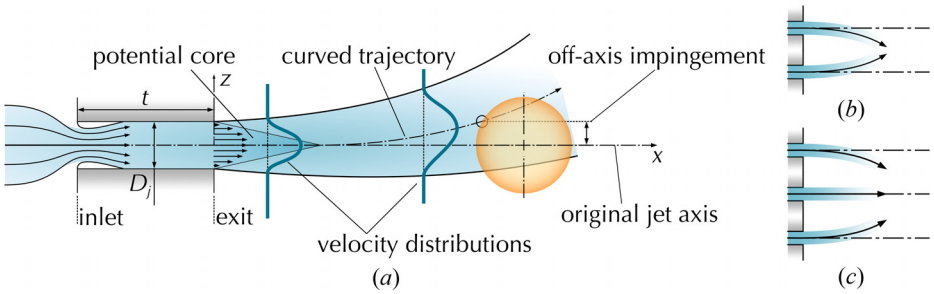


Fig. 3 Flow schematic for a blockage jet exhibiting flow curvature: (*a*) resulting off-axis impingement on a pin-fin, (*b*) mutual entrainment and symmetrical flow curvature, and (*c*) symmetrical entrainment preventing curvature

measurements were undertaken on a simplified configuration of a blockage with perforations that were geometrically aligned with single row of pin-fins and a blockage. Tests were conducted with fully turbulent jet flows ($Re_j = 22{,}000$) observing flows at the end-wall and away from the end-wall, in the midheight plane of the channel (x-z plane), and in the plane of symmetry (x-y plane).

2 Experiment Details

2.1 Test Facility and Setups. The schematic representing the present test setup is displayed in Fig. 4. An axial fan supplies ambient air by a downstream axial fan into a rectangular wind tunnel with cross-sectional dimensions of $W = 400$ mm and $H = 46$ mm. Two perforated blockage plates, with staggered perforations, were installed in the tunnel as shown in Fig. 4. All perforations had the same internal diameter of $D_j = 21$ mm. The blockage plate thickness (t) was half that of the jet diameter (i.e., $t/D_j = 0.5$), which assumes an orifice-type jet flow [23,24]. Two blockages were used as this is considered a more optimal for a blockage pin-fin setup for cooling purposes—the increase in friction factor from an additional blockage is largely negligible [16] while the end-wall heat transfer between the blockages is higher than around a pin-fin array [2,6,16,25], providing more benefit obtained from the additional blockage. As this study is working toward a possible investigation of

Downloaded from http://asmedigitalcollection.asme.org/fluidsengineering/article-pdf/doi/10.1115/1.4064008/7230895/fe_146_05_051302.pdf by The Nanjing University Of Aeronautics & Astronautics user on 18 January 2024

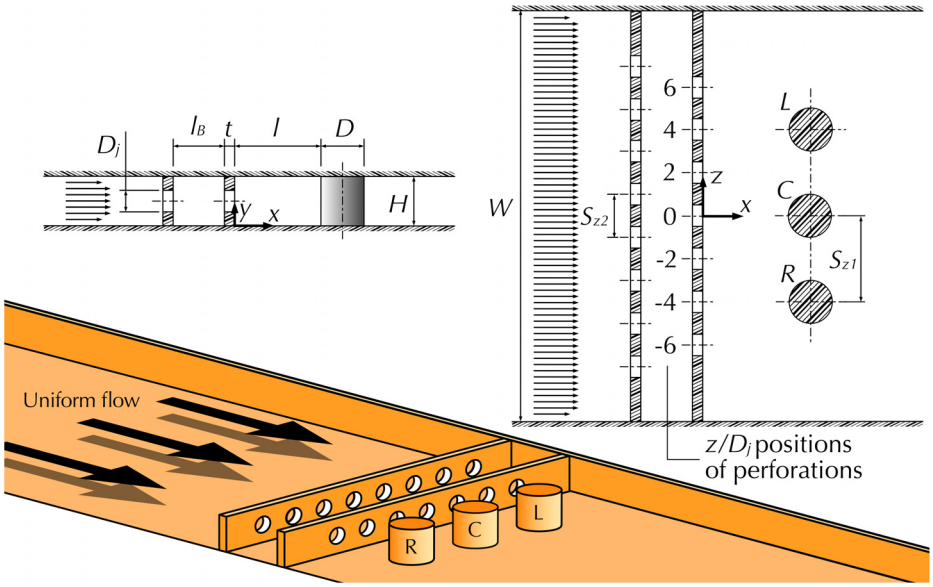


Fig. 4 Cutaway of test setup schematic showing two perforated blockage plates and a single row of three short circular pin-fins with right sidewall and upper end-wall removed

a full blockage pin-fin setup, the decision was made to utilize the double blockage configuration upfront. Perforations were staggered in the spanwise (z-direction) as is conventional for setups using multiple blockages.

Three circular pin-fins were positioned downstream of the second perforated blockage plate. Each pin-fin, denoted as L, C, and R in Fig. 4, had a diameter (D) twice that of the jet diameter (i.e., $D/D_j = 2.0$). The pin-fins had an aspect ratio of $H/D = 1.1$ and a center-to-center spacing of $S_{z1}/D_j = 4.0$ (or $S_{z1}/D = 2.0$). To ensure the alignment of blockage plate perforations with the pin-fins, the perforation spacing (S_{z2}/D_j) was fixed at 2.0. The distance between perforated blockage plates, relative to the height of the channel was kept constant at $l_B/H = 2.0$. The alignment of the pin-fins to the center of the perforation was machined to an accuracy of ± 0.03 mm or 0.3% of the jet diameter (D_j). Perforations in the second blockage plate could be blocked off to control how many jet flows were active into the rear of the channel. The origin of the axis ($x = 0$, $y = 0$, and $z = 0$) was set at the end-wall in the center of the channel, starting from the downstream surface of the second blockage as per Fig. 4.

For any test configuration, the flowrate through the channel was adjusted such that the same Reynolds number based on the jet diameter was maintained at $\mathrm{Re}_j = 2.2 \times 10^4$ (or $\mathrm{Re}_D = 4.4 \times 10^4$ based on pin-fin diameter). A fully turbulent jet would, thus, be expected [26].

Three jet configurations were considered. A 3-jet configuration had only those jets geometrically aligned with the pin-fins being active (the center and outer jets). In a 7-jet configuration, additional jets flanking the sides of the center and outer jets were active. This is equivalent to having a set of jets geometrically aligned with a second row of staggered pin-fins. The terms center, outer, and flanking are used in the discussion of results. The jet configurations and terminology are shown in Table 1. The same perforated blockages are used for all three configurations with the perforations blocked off as necessary.

Table 1 Jet configurations used in the study

Configuration	Active jet axis	Active jets
1-jet	$z/D_j = 0.0$	Center
3-jet	$z/D_j = 0.0, \pm 4.0$	Center and outer
7-jet	$z/D_j = 0.0, \pm 2.0, \pm 4.0, \pm 6.0$	Center, outer, and flanking

As seen in a previous study of a jet impingement with a short pin-fin [5], the potential core length of a given jet was a notable factor. The distance between the jet exit and pin-fin (l/D_j) was set based on the potential core length of the jet with three specific positions: with the pin-fin within the potential core of the jet, with the pin-fin at or near the tip of the potential core and with the pin-fin outside of the potential core length. A potential core length of approximately $l_p/D_j \approx 2.0$ was measured, agreeing with prior studies [23,27]. From this, the three distances selected were thus: $l/D_j = 1.0$, 2.0, and 4.0. For convenience these are hereon referred to as position 1, 2, and 3, respectively.

Off-axis impingement of a blockage jet on a pin-fin, in a blockage pin-fin setup, results in an undesired reduction in end-wall heat transfer. The off-axis impingement arises from the curvature of the orifice jets. As a baseline case, the behavior of a combination of orifice jets without downstream pin-fins was investigated first. This would use the 1-jet, 3-jet, and 7-jet configurations.

The curvature of the orifice jet is to be considered in two ways: (i) the shift of the peak velocity of jet and (ii) the distribution of the flow velocity about this peak as illustrated in Fig. 3(*a*). Velocity distributions would be extracted from PIV measurements. The velocity magnitudes were normalized against the jet exit velocity (v_e). Further, the direction of the flow vectors was assessed. The direction would be obtained by using the component U and V velocity vectors (aligned with the x- and z-axis respectively) and calculating the angle of the resulting vector by $arctan(V/U)$. The direction was then calibrated such that a positive angle implied a flow that was inclined toward the original axis of the jet (at exit). Conversely, a negative angle then implied a flow that was inclined away from the from the central axis of the jet. An angle between 0 deg and 90 deg implied flow in the positive x-direction while an angle above 90 deg implied that the flow was in the negative x-direction or moving upstream.

2.2 Flow Field Mapping Using Particle Image Velocimetry.

The impingement of blockage jets on a pin-fin array was mapped by particle image velocimetry (PIV) as shown in Fig. 5(*a*). The channel could be rotated 90 deg as shown in Fig. 5(*b*) for measurement in the x-y plane. The CCD camera was positioned approximately 500 mm–600 mm above the measurement plane, where the laser light sheet crossed. The camera provided insufficient resolution of the flow field to capture the entire channel width in the x-z plane—instead two measurement windows were used. The first captures just

Downloaded from http://asmedigitalcollection.asme.org/fluidsengineering/article-pdf/doi/10.1115/1.4064008/7230895/fe_146_05_051302.pdf by The Nanjing University Of Aeronautics & Astronautics user on 18 January 2024

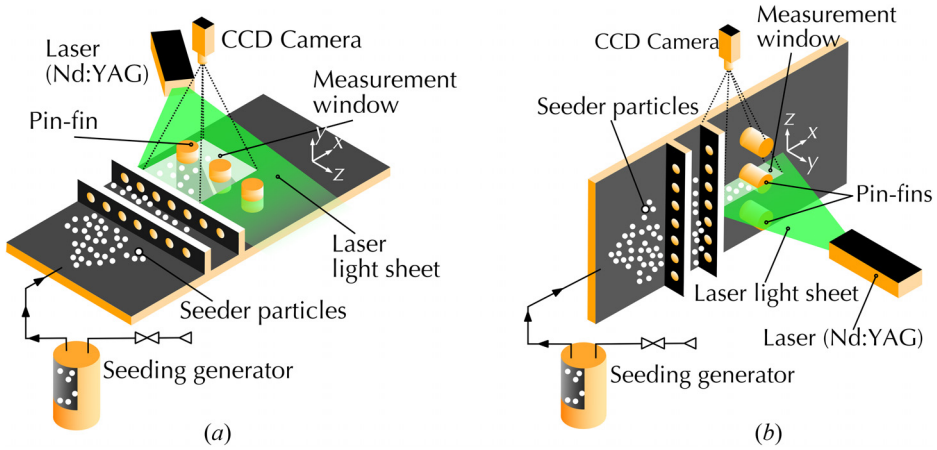


Fig. 5 Particle image velocimetry (PIV) setup for: (*a*) midspan plane illumination and (*b*) plane of symmetry illumination

the C pin-fin and one outer pin-fin (as shown in Fig. 5(*a*)) extending from $-1.0 \leq z/D_j \leq 4.0$. A larger measurement window was used to capture $-5.0 \leq z/D_j \leq 3.0$. The image magnification factor, between object plane (coplanar with the laser light sheet) and image plane of the camera, was of the order of $M_0 \approx 0.1$. Any repositioning of the camera required a recalibration of the setup to obtain the magnification factor.

The larger measurement window was also used to assess symmetry of the flow field about the channel center. From measurements, it was seen that the flow field was suitably symmetrical over the regions being investigated.

The side walls and lid of the test setup were constructed from transparent Perspex to allow for laser illumination and imaging. Clear glass pin-fins were implemented to further increase laser penetration and increase flow illumination between the pin-fins for the midheight plane measurements. This technique, adopted from [28], allowed for the regions that would typically be shadowed by the pin-fins, to be illuminated. Other surfaces were painted in matt black to minimize reflections and light scatter. The jet flow was seeded with an atomized mineral oil (Shell Ondina 901L0996) having a mean particle diameter of approximately 1 μm. The particles were introduced at the inlet to the wind tunnel axial fan. In this way, the particles were evenly distributed through the test section before interacting with the perforated blockages or pin-fins. Review of the images captured during tests was made to ensure an even distribution of particles.

The flow field was illuminated by a pulsed laser light, generated from a frequency-doubled, dual cavity Nd:YAG laser (New Wave Research™), with a light wavelength of 532 nm. When measuring in the x-y plane (Fig. 5(*a*)) the laser was angled such that one pin-fin did not occlude the other which would have reduced the illumination behind the occluded pin-fin too much.

The measurement period is defined by two sequential pulses of the laser light sheet that are separated by a finite time interval—approximately 15–25 μs to ensure a particle displacement $^1/_4$ of the inter-rogation region (16 × 16 pixels). The anticipated displacement of the particle was based on the flow measurements made using a Pitot tube in situ.

The recorded flow field is represented by the random pattern of particle images that are mapped onto the image plane of the CCD sensor. The camera was positioned so the optical axis was perpendicular to and focused on the laser light sheet. The images were recorded on the sensor frame that had a 2048 × 2048-pixel resolution and a pixel pitch of 7.4 μm. The field of view that was setup within the light sheet had a PIV measurement area of the full channel width (200 mm × 200 mm). The PIV images were divided into subregions referred to as inter-rogation areas that were 16 × 16 pixels in size and overlapped by 50%, hence each velocity map contains 255 × 255 vectors and the resulting vector spacing was 0.4 mm. The evaluation of the image field between two successive frames yielded an instantaneous vector map which was achieved with a Dantec Dynamic Studio V1.45 software. The ensemble-averaged velocity field for a specific location in the flow field was then evaluated over an ensemble of 124 instantaneous vector maps sampled at a frequency of 5 Hz. The measurement techniques and setup were based on the work established by Atkins and Kim [28].

2.3 End-Wall Surface Flow Visualization Using an Oil-Dye Mixture Technique. End-wall surface flow pattern was visualized using an oil-dye mixture technique in the wind tunnel. Florescent powder (the dye) was mixed with a light diesel fuel (the oil), and the mixture was then applied to the end-wall surface. When the airflow passes over the end-wall the resulting shear stresses distribute the dye while it is suspended in the diesel. The diesel evaporates and the powder is deposited onto the end-wall surface. The powder creates patterns that represent the end-wall flow patterns present during the test. Validation and interpretation of such topologies have been independently validated against near end-wall PIV measurements in a previous study [5] as well as in comparisons to previous studies of end-wall flows [29]. The visualized flow patterns represent a time-averaged end-wall flow topology. Variations in the flow topologies during a test, from large instabilities, for example, will result in the powder patterns being disrupted in the affected region with no clear streamlines being visible. Areas where the flow is more regular result in finer details. More details associated with this flow visualization technique are found in Kim et al. [30].

2.4 Data Reduction Parameters. Based on centerline velocity of the jet measured at blockage exit (v_e) and blockage perforation diameter (D_j) as the characteristic length, the Reynolds number is defined as

$$\mathrm{Re}_j = \frac{\rho v_e D_j}{\mu} \tag{1}$$

where ρ is the air density in kg/m^3 and μ is the air viscosity in kg/(ms).

Measurement uncertainties were estimated using a method as follows. If $y = f(x_1, x_2, \ldots, x_n)$, then the uncertainty propagated by x_i in the variable y is given by Coleman and Steele [31]

$$\Delta y = \sqrt{\left(\frac{\delta y}{\delta x_1}\Delta x_1\right)^2 + \left(\frac{\delta y}{\delta x_2}\Delta x_2\right)^2 + \cdots + \left(\frac{\delta y}{\delta x_n}\Delta x_n\right)^2} \tag{2}$$

Using this method, the uncertainty associated with the Reynolds number was calculated to be within 1.8%. The uncertainty of the

Downloaded from http://asmedigitalcollection.asme.org/fluidsengineering/article-pdf/doi/10.1115/1.4064008/7230895/fe_146_05_051302.pdf by The Nanjing University Of Aeronautics & Astronautics user on 18 January 2024

instantaneous PIV velocity was estimated based on the contributions of the mean bias and random errors present during PIV interrogations. Westerweel [32] showed that the random measurement errors are directly proportional to the particle image diameter and are a function of the number of particle images within the interrogation area, and subpixel displacements. In addition, background noise contributes to the random error. Taking these factors into consideration the random error is estimated to be 0.17 pixels, based on an average particle image diameter of 2.8 pixels. The particle image diameter was measured using the autocorrelation of the PIV recordings, where the resulting self-correlation peak width is $2^{1/2}$ times the particle image diameter. This method to determine the particle image diameter was preferred to the analytical diffraction-limited spot size estimation, that tends to underestimate the value due to nonideal performance of the lens and imaging arrangement. The ideal number of particle image pairs (10) for the displacement-correlation was assumed according to Adrian and Westerweel [33], based on the high valid vector detection percentage (i.e., ~98%), with ~1000 vectors being rejected out of ~55000 valid vectors detected with 8300 masked vectors. The bias error was shown by Westerweel [34] to be a function of the displacement correlation peak width. The present bias error was estimated to be 0.06 pixels. Therefore, the total measurement uncertainty was determined to be 3.4% based on the valid full-scale displacements of 6.4 pixels, where the total bias and random errors are combined by using the root-sum-square of these terms.

3 Discussion of Results

3.1 The Curvature of Orifice Jets Without Downstream Pin-Fins. The velocity contours from PIV measurements in the midheight plane ($y/H = 0.5$) and without downstream pin-fins are shown in Fig. 6. For a 1-jet configuration (Fig. 6(*a*)), no significant curvature of the jet is observed. With the introduction of additional jets (Figs. 6(*b*) and 6(*c*)), the center jet (exiting at $z/D_j = 0.0$) remains relatively straight. There is a small amount of curvature in the positive z-direction. Away from the channel centerline, however, a notable curvature of the other jets is seen. With the 3-jet configuration, a greater degree of jet curvature of the outer jet, exiting at $z/D_j = -4.0$, is noted. The noted jet curvature would result in the L and R pin-fins being exposed to different flows if present. The difference depends on both the distance between the blockage and pin-fin (l/D_j) and the number of active jets.

Velocity values were extracted from PIV at $\Delta x/D_j = 0.25$ upstream of the equivalent pin-fin positions 1, 2, and 3 (or $x/D_j = 0.75$, 1.75, and 3.75). These were used to calculate the distribution of the velocity magnitudes (Fig. 7(*a*)) and flow direction (Fig. 7(*b*)) about $z/D_j = 0.0$ and -4.0. These z-direction positions correlate with the original axis of the center and outer jets, respectively.

The velocity magnitude distribution of the center jet is predominantly similar at all positions as seen by Fig. 7(*a*: i–iii) for 1-, 3-, and 7-jet configurations—at least within the equivalent

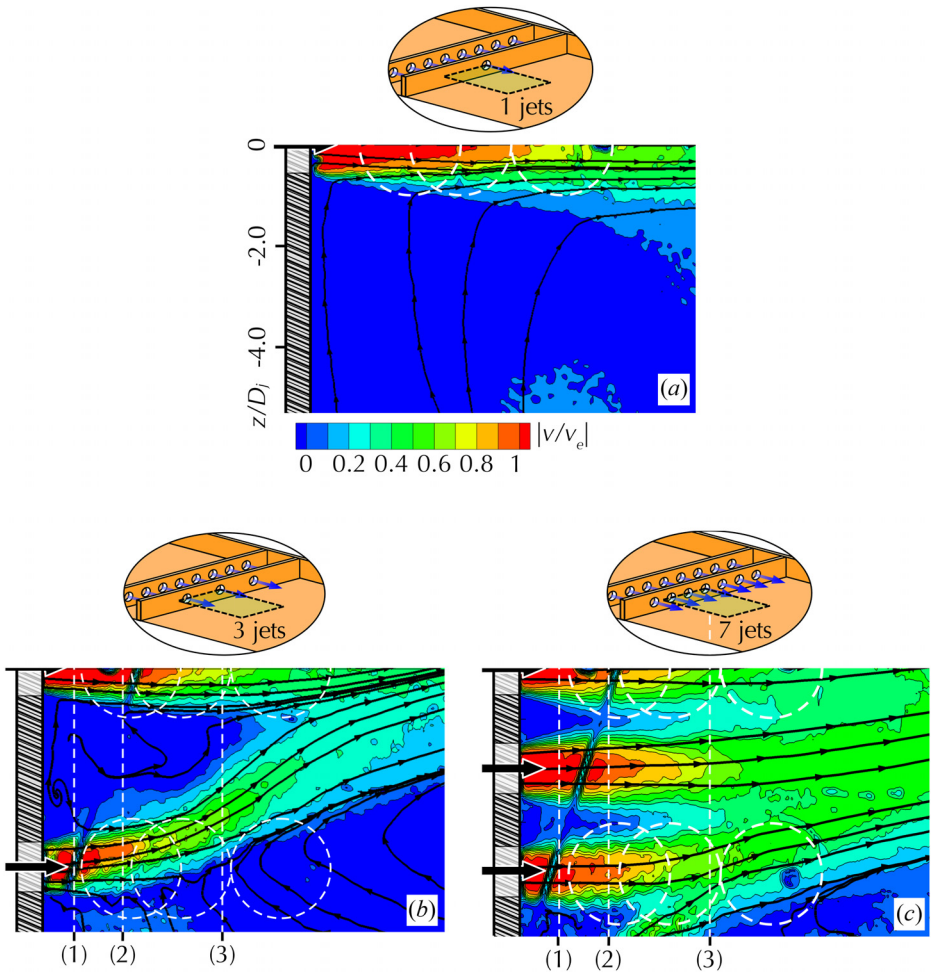


Fig. 6 PIV velocity contours in the midheight plane ($y/H = 0.5$) comparing three configurations of orifice jets exiting in an empty channel at $Re_j = 22{,}000$: (*a*) for a single 1-jet configuration, (*b*) for a 3-jet configuration, and (*c*) for a 7-jet configuration

Downloaded from http://asmedigitalcollection.asme.org/fluidsengineering/article-pdf/doi/10.1115/1.4064008/7230895/fe_146_05_051302.pdf by The Nanjing University Of Aeronautics & Astronautics user on 18 January 2024

boundary of the pin-fin ($-1.0 \leq z/D_j \leq 1.0$). With the 7-jet configuration, however, there is a notably larger amount of flow at the periphery of the jet. This is due to the close proximity of the flanking jets exiting at $z/D_j = \pm 2.0$. The flow direction distributions of the center jet are not similar for 1-, 3- and 7-jet configurations. But they are predominantly symmetrical about the jet's original axis (Fig. 7(*b*: i–iii)). The slight curvature of the center jet is noted in Figs. 6(*b*) and 6(*c*) are not discernible at position 1 or 2 with the flow direction distributions remaining symmetrical. At position 3 (Fig. 7(*b*: iii)), however, the distributions are asymmetric for the 1- and 3-jet configurations by the jet periphery. The velocity magnitudes (Fig. 7(*a*: iii)) are low ($|v/v_e| < 0.1$). Within the equivalent diameter of the pin-fin ($-1.0 \leq z/D_j \leq 1.0$), the flow direction is skewed by only 1 deg–3 deg in the positive z-direction. The curvature noted in Fig. 6 is thus taken as sufficiently inconsequential.

The velocity distributions for the outer jet are also similar for 3- and 7-jet configurations in position 1 (Fig. 7(*a*: iv). The flow directions (Fig. 7(*b*: iv)) do not appear similar. However, there is a much larger change in flow direction at the periphery of the outer jet in the 3-jet configuration. But this is misleading as the low flow velocity in this same region indicates that the differences are less consequential. It is necessary to consider both the velocity magnitude and direction. By position 2, however, the position of the peak velocity for the 3-jet configuration has shifted to $z/D_j = -3.6$ (Fig. 7(*a*: v)), and the distribution has become asymmetric. Notably, however, the flow direction distribution between the 3- and 7-jet configurations appears to correlate better in position 2. At the position of peak velocity magnitude for the 3-jet configuration, the flow direction is approximately −13 deg (Fig. 7(*b*: v)). By position 3, there is no significant flow for $z/D_j \leq -4.0$ with the 3-jet configuration—the peak velocity skewed to $z/D_j = -3.0$ (Fig. 7(*a*: vi)). At that position, the flow direction is −30 deg (Fig. 7(*b*: vi)). A pin-fin in position 3 may then have no flow impinging on its outer side with a 3-jet configuration.

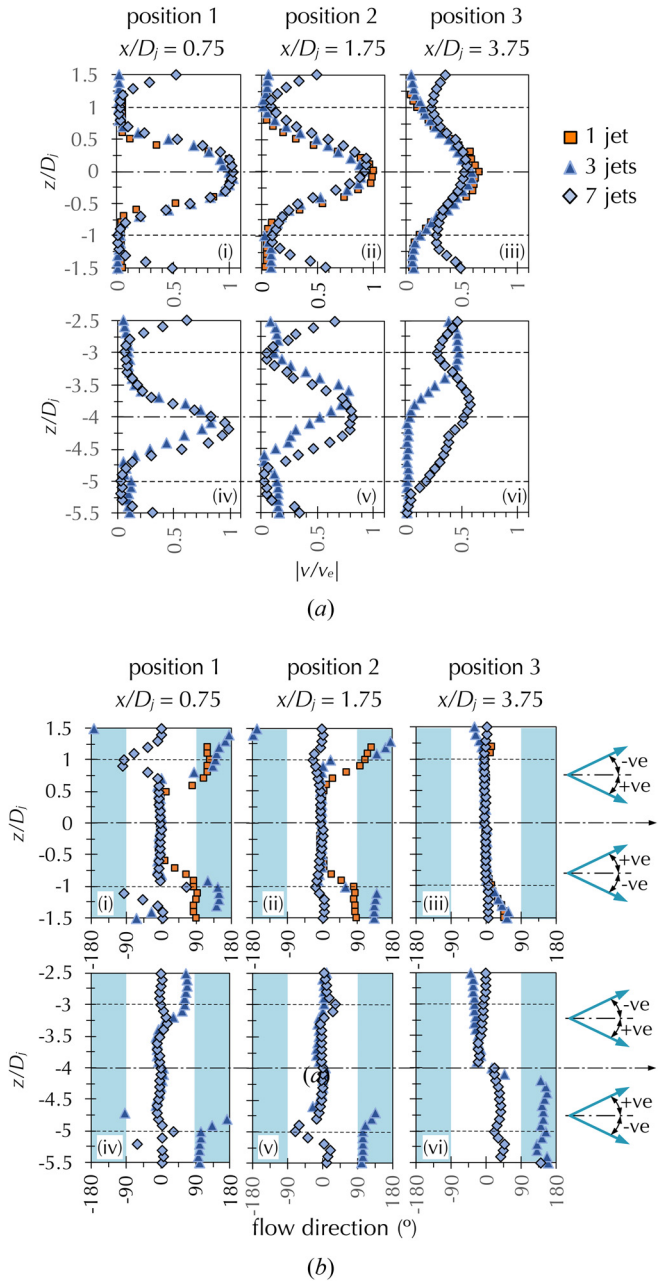


Fig. 7 Distribution of flow direction along the jet axis for the center jet (at $z/D_j = 0.0$) and outer jet (at $z/D_j = -4.0$) for $x/D_j = 0.75$, 1.75, and 3.75 for orifice jets exiting into empty channel at $Re_j = 22{,}000$

Downloaded from http://asmedigitalcollection.asme.org/fluidsengineering/article-pdf/doi/10.1115/1.4064008/7230895/fe_146_05_051302.pdf by The Nanjing University Of Aeronautics & Astronautics user on 18 January 2024

The additional jets and smaller transverse spacing of the 7-jet configuration reduce the curvature of the outer jet in Fig. 6(*c*). By position 2, the peak velocity remains at $z/D_j = -4.0$ (Fig. 7(*a*: v) and the velocity distribution is largely symmetrical. Further, the flow direction is < 1 deg in this region (Fig. 7(*b*: v)). By position 3, however, the peak velocity has shifted to $z/D_j = -3.8$ and the distribution has become asymmetrical. There is a much larger proportion of flow at $-2.5 \le z/D_j \le -4.0$ compared to $-4.0 \le z/D_j \le -5.5$. The flow direction, at the position of peak velocity, is approximately −19 deg and the majority of flow has a component inclined toward the channel center (Fig. 7(*b*: vi). Note that, as shown in Fig. 6(*c*), the flanking jet (exiting at $z/D_j = -6.0$) has already merged with the outer jet (exiting at $z/D_j = -4.0$) by position 3. Very little flow exists at the outer periphery ($z/D_j \le 4.5$) of the outer jet of a 7-jet configuration in position 3.

3.2 Effect of Pin-Fins on Orifice Jet Curvature. The velocity contours from PIV of the orifice jets interacting with pin-fins in various configurations are shown in Fig. 8. In all four configurations shown, the center jet (exiting at $z/D_j = 0.0$) appears to continue exhibiting a negligible curvature. Through comparisons to the velocity contours without pin-fins (Fig. 6), the jet exiting at $z/D_j = 4.0$ continues to curve for the 3-jet configuration (Figs. 8(*b*) and 8(*c*)). The curvature for the 7-jet configuration (Fig. 8(*d*)), however, appears to be manipulated to some degree. Further, a vortical type flow is formed by the L pin-fin for the 3-jet configurations at positions 2 and 3 (Figs. 8(*b*) and 8(*c*)). Such a vortical structure can be observed in the numerical results of Kan et al. [2].

With the pin-fins at position 1 (Fig. 8(*a*)), there is insufficient distance for the jets to notably curve before impingement. There were no significant changes to the velocity magnitude and flow

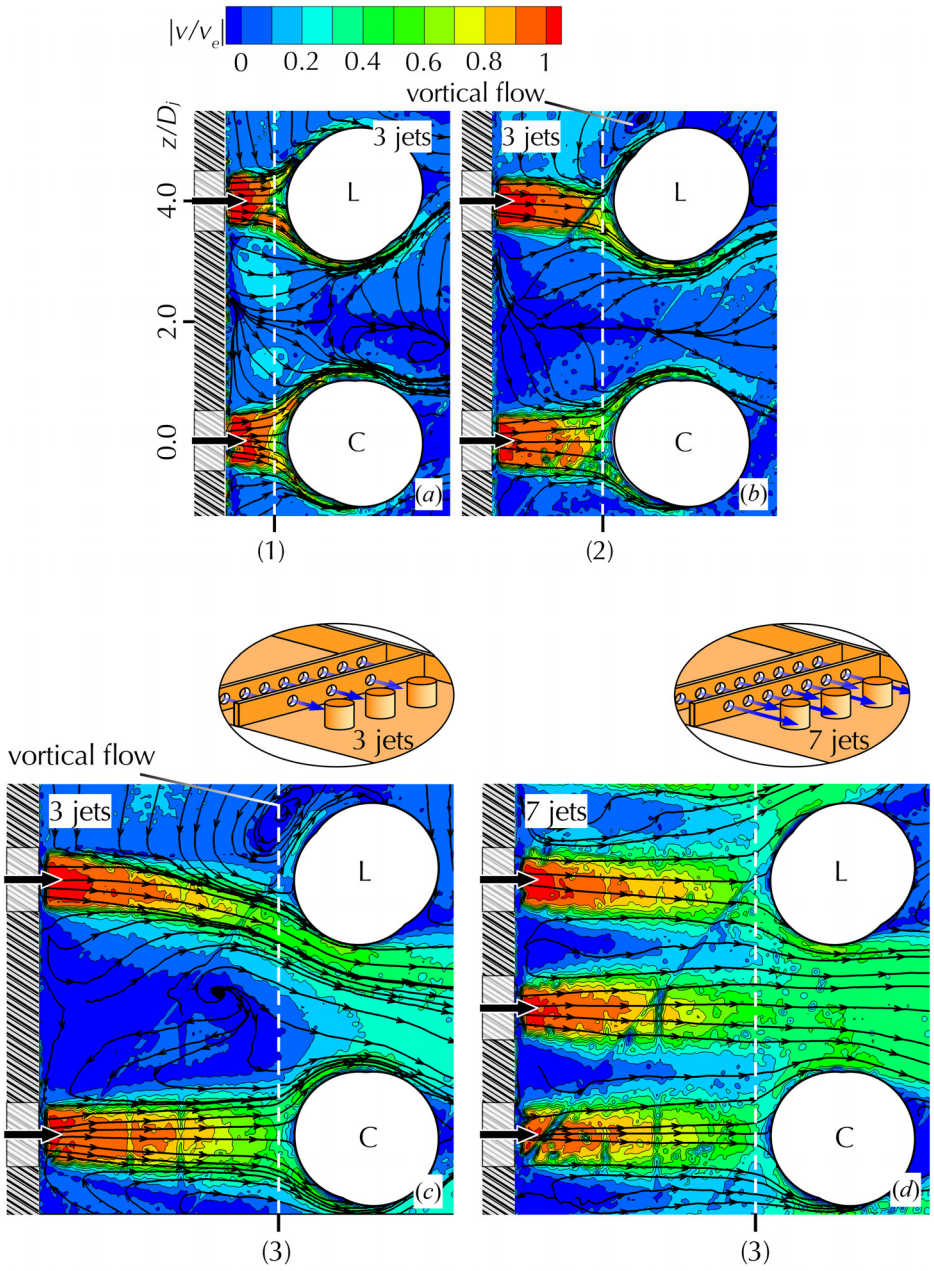


Fig. 8 Velocity contours in the midheight plane ($y/H = 0.5$) from PIV at $Re_j = 22{,}000$: (*a*) for a 3-jet configuration with a blockage-to-pin spacing of $l/D_j = 1.0$, (*b*) for a 3-jet configuration with a blockage-to-pin spacing of $l/D_j = 2.0$, (*c*) for a 3-jet configuration with a blockage-to-pin spacing of $l/D_j = 4.0$, and (*d*) for a 7-jet configuration with a blockage-to-pin spacing of $l/D_j = 4.0$

Downloaded from http://asmedigitalcollection.asme.org/fluidsengineering/article-pdf/doi/10.1115/1.4064008/7230895/fe_146_05_051302.pdf by The Nanjing University Of Aeronautics & Astronautics user on 18 January 2024

direction distributions for position 1 with the pin-fins in place. This was similar to position 2 with the 3-jet configuration (Figs. 9(i) and 10(i)). At position 3, however, the peak velocity remains skewed toward the center of the channel but there is a sharper peak velocity with the pin-fin in place—the distribution toward the outer side of the channel remains the same. Further, the flow direction distributions become reversed in the region $4.0 \leq z/D_j \leq 5.0$ with the pin-fins in place (Fig. 10(ii)). Specifically, the flow in this region changes from being consistently toward the center of the channel to predominantly away from the channel center. This inclination is approximately 45 deg, although it is as much as 65 deg at the center of the pin-fin ($z/D_j = 4.0$). This is due to the circumferential flow around the surface of the L pin-fin (seen in Fig. 8(*b*)) redirecting the flow outwards away from the channel center. The velocity magnitudes are very low in this region and so the large change in flow direction is misleading. The presence of the pin-fin can then be considered to have a negligible effect on the jet curvature for the 3-jet configuration. There exists an asymmetrical flow field interacting with the pin-fin at positions 2 and 3.

For the 7-jet configuration, the peak velocity magnitudes for the outer jet are further skewed toward the center of the channel (Fig. 9(iii, iv)). For position 2 (Fig. 9(iii)) the position of the peak velocity in the z-direction approximately matches that of the 3-jet configuration—being $z/D_j = 3.6$ (in Fig. 9(i)). Without the pin-fin, the outer jet curved less due to the entraining action by the flanking jet exiting at $z/D_j = 6.0$. With the pin-fin in place, this corrective action is seemingly reduced, and the outer jet is able to curve more. This change is also seen in the flow direction distribution (Fig. 10(iii)) in the range $4.0 < z/D_j < 5.0$. At position 3 the peak velocity of the outer jet has also moved further toward the channel center compared to when there is no pin-fin. But the peak position is similar to that for position 2 (at $z/D_j = 3.5$). Notably, however, a larger velocity magnitude is present at the periphery ($5.0 \leq z/D_j \leq 5.5$) due to the presence of the same flanking jet. Without the pin-fin, this latter jet curves and merges with the flow of the outer jet before position 3 (Fig. 6(*c*)). The pin-fin is thus acting to inhibit the curvature of the jet. Within the diameter of the pin-fin (between $3.0 \leq z/D_j \leq 5.0$), however, the pin-fin is actually exposed to an overall lower velocity magnitude than what exists without the pin-fin in place. This may in part be due to the jet decelerating before impingement. Considering both velocity magnitude and flow direction (Figs. 9(iv) and 10), the L pin-fin is exposed to a more symmetrical flow at position 3. At position 2, however, the pin-fin remains exposed to an asymmetrical flow, similar to the 3-jet configuration.

For the center jet (at $z/D_j = 0.0$), the velocity magnitude and flow direction distributions are mostly unchanged when the pin-fins are introduced (Figs. 9(v–viii) and 10(v–viii)). The peak velocity near the core of the jet is lower with pin-fins due to the jet decelerating as it stagnates on the pin-fin. The pin-fins therefore have a largely negligible effect on the curvature of the orifice jets leading up to impingement. This may not hold for large blockage to pin-fin distances (l/D_j). Such larger distances result in the pin-fin being exposed to an overall lower jet velocity magnitude. In turn, this results in weaker end-wall flow and corresponding weaker end-wall heat transfer.

3.3 The Interactions of End-Wall Flow for a Singular Pin-Fin. Two distinct interactions of end-wall flows for pin-fins subjected to jet impingement are of interest. The primary interaction is between the pin-fins (marked in Fig. 2(*d*)). The other interaction is between the end-wall flows and the upstream perforated blockage. To first isolate these effects, the end-wall flows around a singular pin-fin subjected to a single jet impingement was investigated as shown in Fig. 11. As a reference, Fig. 11(*a*) shows the PIV measurement (top) taken at $y/H = 0.08$ and end-wall oil-dye measurement (bottom) for a fully developed jet (formed by a long tube) impinging on a pin-fin. The jet impinges on the pin-fin at its midspan ($y/H = 0.5$). Wall-jet flows are directed along and around the pin-fins, some of which contact the end-wall. These flows then are forced to radiate outwards from the pin-fin surface. From the leading-edge of the pin-fin, the end-wall flows fan out radially until becoming tangential to the pin-fin surface. All flows away from the leading-edge are similarly tangential to the pin-fin. These observations of flow profiles and vectors were interpreted in the oil-dye patterns and confirmed by the PIV measurement.

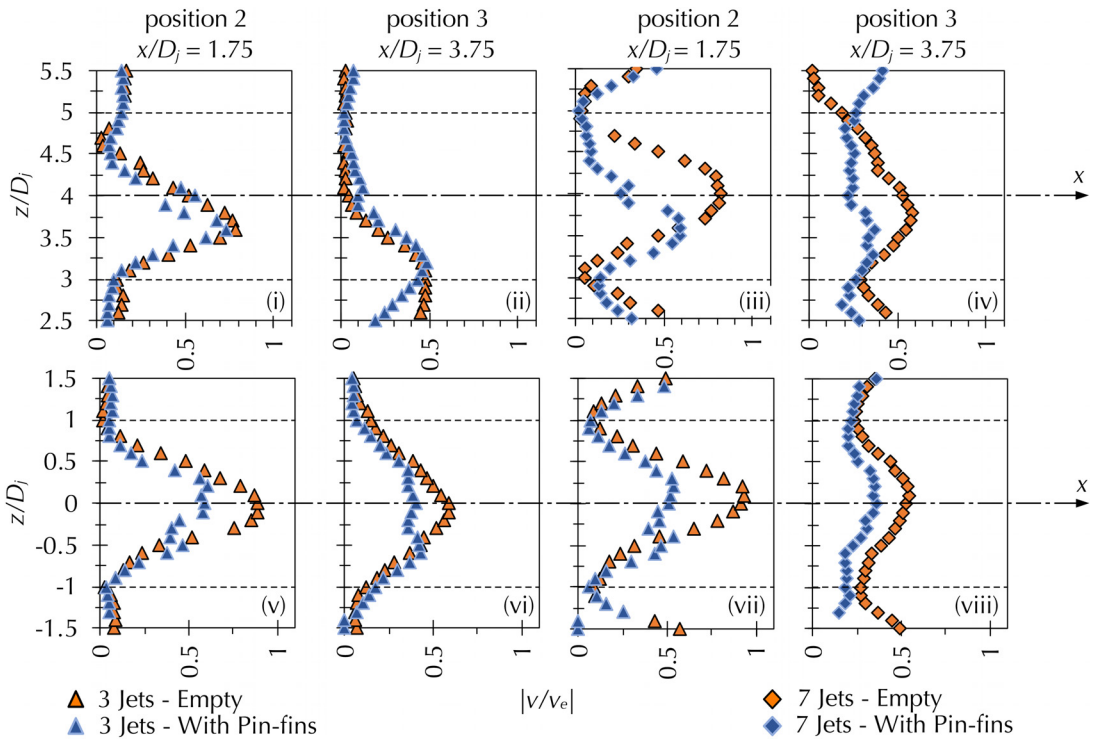


Fig. 9 Extracted velocity distributions in the midheight plane ($y/H = 0.5$) along the z-axis at $\Delta x/D_j = 0.25$ upstream of the pin-fin at $Re_j = 22{,}000$ for 3-jet and 7-jet configurations

Downloaded from http://asmedigitalcollection.asme.org/fluidsengineering/article-pdf/doi/10.1115/1.4064008/7230895/fe_146_05_051302.pdf by The Nanjing University Of Aeronautics & Astronautics user on 18 January 2024

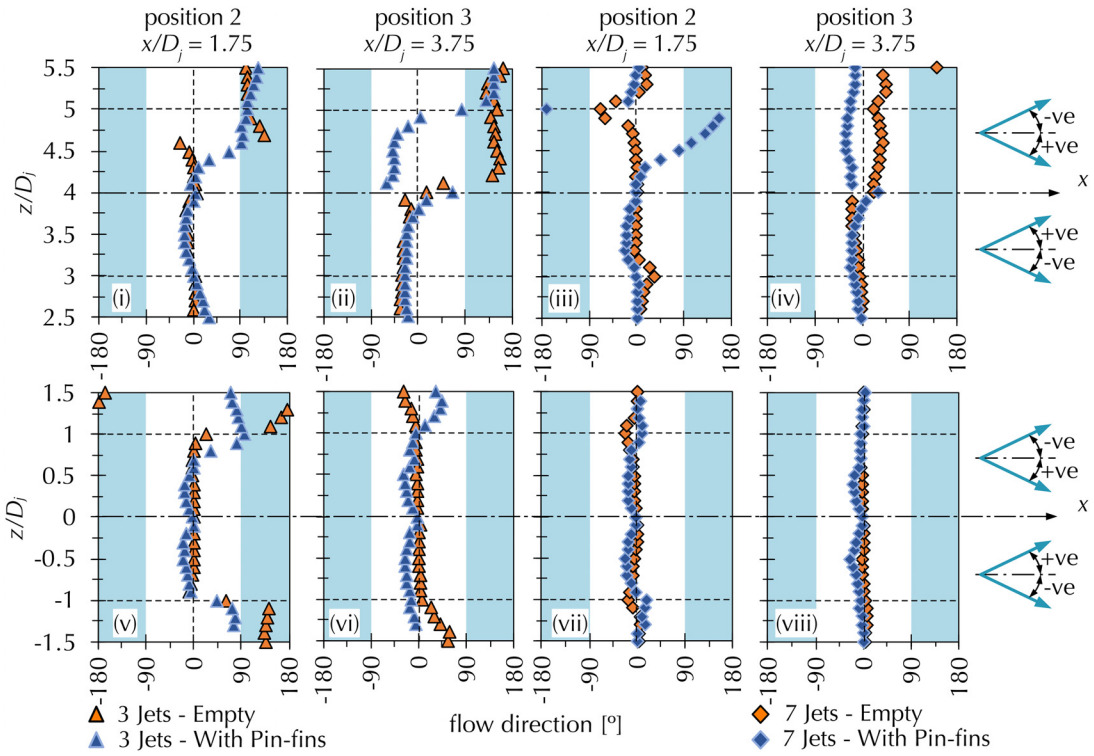


Fig. 10 Extracted flow direction distributions in the midheight plane ($y/H = 0.5$) along the z-axis at $\Delta x/D_j = 0.25$ upstream of the pin-fin at $Re_j = 22{,}000$ for 3-jet and 7-jet configurations

An upstream perforated blockage forming an orifice jet, instead of the fully developed jet, causes the end-wall profiles as shown in Figs. 11(*b*) and 11(*c*). For position 1 (Fig. 11(*b*)), the front end-wall flow pattern (marked by the dotted line) is deformed, being conformal to the blockage surface. The deformation demonstrates a notable amount of flow interaction with the surface of the perforated blockage. The perforated blockage redirects the end-wall flow upwards, away from the end-wall (in the y-direction) toward the jet exit, and incites a vortical flow in the x-y plane (Fig. 12(*a*)). The circulating flow occurs without the blockage in Fig. 12(*b*), but the

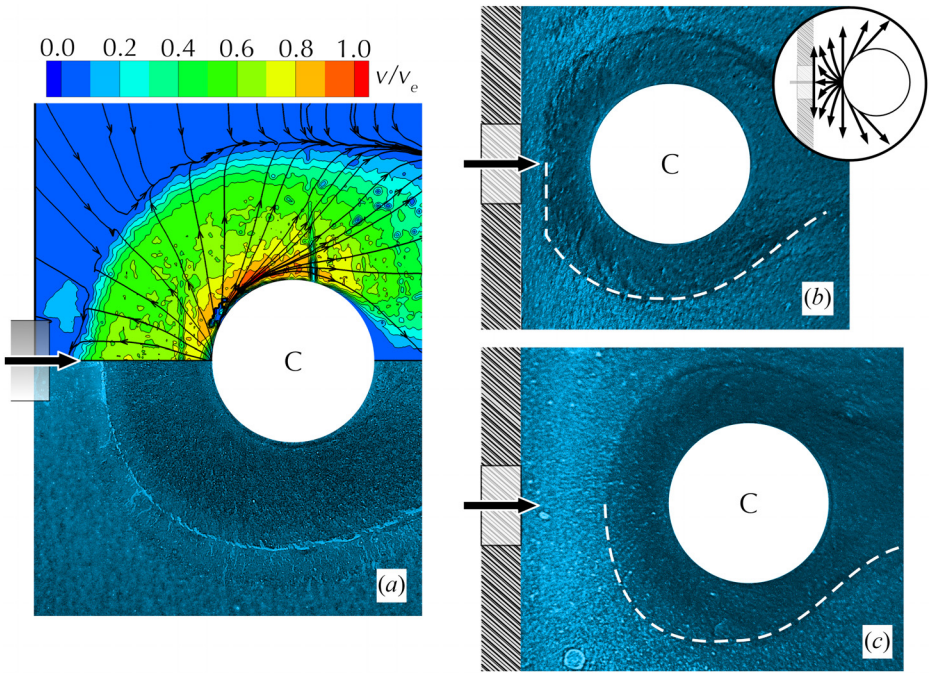


Fig. 11 End-wall flows around a single pin-fin subjected to jet impingement: (*a*) velocity contours from PIV at $y/H = 0.08$ (top) and oil-dye flow visualization (bottom) for a tube jet positioned at $l/D_j = 2.0$ for $Re_j = 17{,}500$, (*b*) oil-dye flow visualization for an orifice jet positioned at $l/D_j = 1.0$ for $Re_j = 22{,}000$ with flow schematic (inset), and (*c*) oil-dye flow visualization for an orifice jet positioned at $l/D_j = 2.0$ for $Re_j = 22{,}000$

Downloaded from http://asmedigitalcollection.asme.org/fluidsengineering/article-pdf/doi/10.1115/1.4064008/7230895/fe_146_05_051302.pdf by The Nanjing University Of Aeronautics & Astronautics user on 18 January 2024

blockage constrains the flow and redirects it. Note that this redirection is both upwards and away from the end-wall surface (Fig. 12(*a*) but also be outwards in a spanwise (*z*)-direction (as illustrated by the inset of Fig. 11(*b*)), along the blockage surface.

At position 2 (Fig. 11(*c*)) the front pattern of the end-wall flow is far less deformed. The velocity contours in the *x*-*y* plane (Fig. 12(*c*)) show flow along the surface of the blockage, more than the same relative location without the blockage in Fig. 12(*b*). The interactions are thus still occurring at position 2 although they have a less notable effect on the end-wall flow pattern around the pin-fin. At $l/D_j = 2.0$ both the tube jet (Figs. 11(*a*) and 12(*b*)) and orifice jet (Figs. 11(*c*) and 12(*c*)) have largely similar topologies for the observed flows, as expected. Those differences that exist are attributed more to the presence of the upstream blockage instead of the behavior of the jet flow itself.

The flow along the downstream surface of the perforated blockage may result in improved cooling of that structure in the flow. The contribution of the perforated blockage to the overall cooling performance has not been directly considered in prior studies of either perforated blockage or blockage pin-fin setups.

3.4 The Interactions of End-Wall Flow for Multiple Pin-Fins. The effect of multiple pin-fins on the end-wall flow patterns is seen in Fig. 13. The end-wall flow patterns around three pin-fins subjected to a uniform-like flow is used as reference (Fig. 13(*a*)). There, the horseshoe vortex patterns are similar to each other, being of equal size and shape. Between the pin-fins, streamlines are focused into a narrow band and directed downstream. Overall, the distinct horseshoe vortex patterns maintain their characteristic features when neighboring pin-fins are present, similar to the that shown in Fig. 2(*c*) based on prior studies.

With multiple pin-fins subjected to impinging orifice jets, the end-wall flow patterns vary distinctly. Consider first the end-wall patterns for position 1 (Fig. 13(*b*)). At this pin-fin position, there was minimal jet curvature noted and relatively symmetrical flow around the pin-fin in the midheight plane (Fig. 8(*a*)). There is then expected to be minimal effects of flow curvature present. The end-wall flow patterns can be taken as representing the base end-wall flow interactions.

The primary interaction noted is between the L and C pin-fins where the end-wall flow radiating from the pin-fins intersect (as per Fig. 2(*b*)). Rather than a band of focused but clear streamlines between the pin-fins as seen in Fig. 13(*a*), there is a band of disrupted dye pattern with no clear streamlines in Fig. 13(*b*). This "band of disrupted flow" continues downstream. A staggered second row of pin-fins would thus have a region of end-wall flow interacting with it. The band of disrupted flow also extends all the way upstream to the blockage surface. Near the blockage, the flows along its surface (as illustrated in the inset of Fig. 9(*b*)), contribute to the band of disrupted flow. Downstream of the pin-fins, the band of disrupted flow prevents the convergence of the flow in the wake of the pin-fins. This is in contrast to a conventional pin-fin array (Figs. 2(*c*) and 13(*a*)) that continues to feature converging wake flows when neighboring pin-fins are present. Further, in the midheight of the channel the upstream pin-fin row blocks the jet flows from reaching the second row directly. The lack of convergence in the wake then prevents flows from reaching the second row of pin-fins. With an inline second row of pin-fins the pin-fins would likely be exposed to very little flow. A staggered row of pin-fins has been determined to be more effective for conventional pin-fin arrays and was used in prior studies of blockage pin-fin setups [2,3]. This is confirmed to then be appropriate and necessary for an optimal blockage pin-fin setup.

The end-wall flow profiles around the outer pin-fins (L and R) vary distinctly from those in Figs. 11(*b*) and 11(*c*) at both position 1 and 2—being asymmetric. For position 1 (Fig. 13(*b*)), the pattern appears skewed toward the center of the channel. This asymmetry may be due to the lack of any flow from the outer side of the pin-fin (from the channel wall). It is unlikely to be attributed to asymmetry in the flow direction of the outer jet (exiting at $z/D_j = \pm 4.0$). Thus, a similar asymmetry would be expected at position 2 (Fig. 13(*c*)). However, the asymmetry presents differently: the front of the pattern is not flattened due to the larger l/D_j spacing (similar to that for the singular pin-fin in Fig. 9(*c*)) and it is also not skewed, appearing more symmetrical about the L pin-fin. Asymmetry is in the form of the vortical structure forming off the outer leading-edge.

For a 7-jet configuration at position 2 (Fig. 13(*d*)), the flow pattern is again asymmetrical but with the pattern skewed toward the sidewall of the channel (away from the center). This can be understood by comparing the velocity magnitudes and flow direction between the 3-jet and 7-jet configurations in Figs. 9(i, iii) and 10(i, iii). In both configurations the peak velocity magnitudes are very similarly skewed toward the center of the channel and the flow direction on the inner side of the pin-fins is similar. For the 7-jet configuration, there is a notable amount of flow from the flanking jet exiting at $z/D_j = 6.0$. This jet causes the flow in that region ($5 \leq z/D_j \leq 5.5$) to have a direction toward the pin-fin rather than away from it.

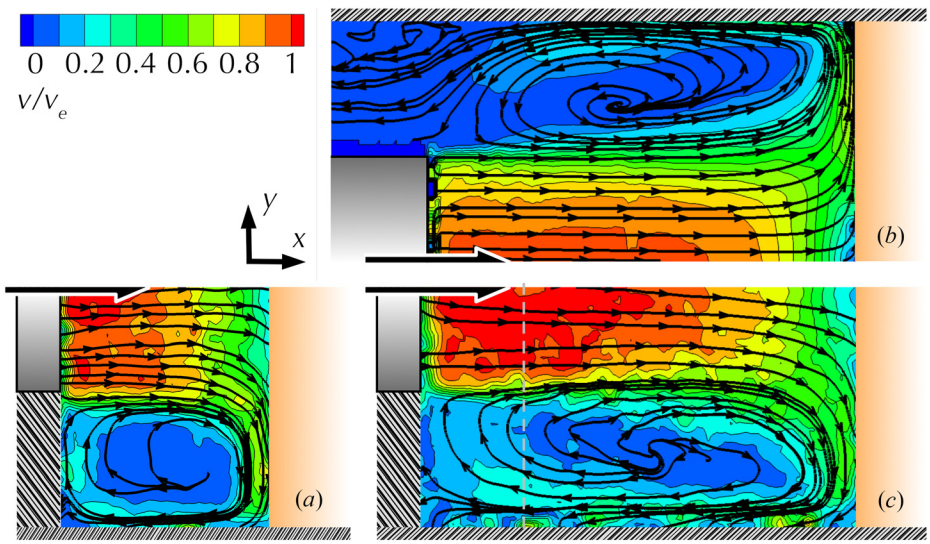


Fig. 12 Flow field in the plane of symmetry (*x*-*y* plane) of a single pin-fin subjected to an impinging jet: (*a*) for $l/D_j = 1.0$ with an orifice jet at $Re_j = 22{,}000$, (*b*) for $l/D_j = 2.0$ with a tube jet at $Re_j = 17{,}500$, and (*c*) for $l/D_j = 2.0$ with an orifice jet at $Re_j = 22{,}000$

Downloaded from http://asmedigitalcollection.asme.org/fluidsengineering/article-pdf/doi/10.1115/1.4064008/7230895/fe_146_05_051302.pdf by The Nanjing University Of Aeronautics & Astronautics user on 18 January 2024

Further, this flanking jet results in additional flow interacting with the outer side of the pin-fin surface. This is sufficient to result in there being a larger amount of end-wall flow around the outer side of the L pin-fin and the distortion of the flow pattern as seen in Fig. 13(*d*). Further, the flow pattern around the C pin-fin in the 7-jet configuration is subtly changed compared to the 3-jet configuration. The front profile is flatter indicating an increase in the amount of flow in the region.

The impact of this additional flow from the flanking jets exiting at $z/D_j = \pm 2.0$ and ± 6.0 is even more clearly seen at position 3 in Figs. 13(*e*) and 13(*f*). In the midheight plane, there is a lower velocity magnitude interacting with the pin-fins (as per Figs. 9(ii, iv, vi, viii)). This results in weaker end-wall flows that are less distinguishable in the dye patterns as seen in Figs. 13(*e*) and 13(*f*). The patterns were much clearer for the 7-jet configuration (Fig. 13(*f*)) compared to the 3-jet configuration (Fig. 13(*e*)). The latter only exhibited an ambiguous pattern around the C pin-fin. The stronger end-wall flows of the 7-jet configuration are then attributed to the lessened curvature of the outer jet in the midheight plane. This variation in jet curvature between 3- and 7-jet configurations presents as follows. The velocity distribution is better spread over the diameter of the pin-fin ($3.0 \leq z/D_j \leq 5.0$) for the 7-jet configuration (Fig. 9(iv)). For the 3-jet configuration, the outer jet is focused entirely on the inner side of the L pin-fin ($3.0 \leq z/D_j \leq 4.0$ in Fig. 9(ii)). The average



Fig. 13 Close up end-wall flow fields from oil-dye with 3 pin-fins for $Re_j = 22{,}000$ ($Re_D = 44{,}000$) with overviews as inset: (*a*) with a uniform like flow interacting with the pin-fins, (*b*) for position 1 with a 3-jet configuration, (*c*) for position 2 with a 3-jet configuration, (*d*) for position 2 with a 7-jet configuration, (*e*) for position 3 with a 3-jet configuration, and (*f*) for position 3 with a 7-jet configuration

Downloaded from http://asmedigitalcollection.asme.org/fluidsengineering/article-pdf/doi/10.1115/1.4064008/7230895/fe_146_05_051302.pdf by The Nanjing University Of Aeronautics & Astronautics user on 18 January 2024

velocity magnitude ($|v/v_e|$) across the pin-fin diameter is 0.27 for the 7-jet configuration (Fig. 9(iv)) while it is 0.19 for the 3-jet configuration (Fig. 9(ii)) despite the peak velocity being higher. Further, the flow direction over this range is almost symmetrical about the pin-fin axis ($z/D_j = 4.0$)—with flows consistently directed away from the axis—for the 7-jet configuration (Fig. 10(iv)). The flow direction is, however, asymmetrical for the 3-jet configuration (Fig. 10(ii))—consistently toward the channel center to a varying degree. The reduced curvature in the 7-jet configuration is attributed to the presence of the flanking jets. While these are not directly impinging on the pin-fin, they inhibit flow curvature. The outer jet then still impinges on the pin-fin both with a higher average velocity and a more symmetrical flow inclination (Fig. 10(iv)). The result is an end-wall flow pattern around the L pin-fin that is almost symmetrical and of greater definition (Fig. 13(*f*)).

Regardless, the large distances of position 3 are likely to result in too low end-wall heat transfer. There is also less flow interacting with the downstream surface of the perforated blockage which, in turn, would result in an overall poorer cooling performance. An optimal setup should position the first row of pin-fins at least at position 2. Further, a 7-jet configuration (featuring flanking jets) is strongly recommended. The flanking jets can prevent flow curvature and provide a more symmetrical flow field (by way of flow inclination) and higher average velocity interacting with the pin-fin. Even in the event that the flanking jets have decelerated before reaching the second row of pin-fins (resulting in equally weak end-wall flows as seen in Figs. 13(*e*) and 13(*f*)) they still serve a useful purpose.

4 Conclusions

This study has investigated the interaction of orifice jets, ejecting into a narrow rectangular channel, with downstream pin-fins. Such an interaction exhibits behaviors not clearly demonstrated in previous studies. Flow fields in the midheight plane, vertical plane, and at the end-wall were considered. Two jet configurations were considered, either having only those jets geometrically aligned with the pin-fins active (three in total) or additional jets flanking the pin-fins (seven in total). Further, distances between the pin-fins and perforated blockages were considered. Measurements utilized a combination of PIV measurements and end-wall flow visualizations. The conclusions of this study are as follows.

A row of orifice jets may be expected to converge downstream. In doing so, each jet except a centrally positioned jet exhibits curvature with the more outer jets having a higher curvature. Curvature presents as both a shift in the peak velocity magnitude toward the center of the channel and an inclination of the flow direction toward the center of the channel. The curvature can be sufficient such that the position of peak velocity magnitude skews in the spanwise direction by as much as half the diameter of the pin-fin. Further, the flow can be inclined as much as 45 deg–60 deg from its original trajectory before impinging on the pin-fins. With flanking jets, resulting in a closer transverse spacing of the jets, the jet curvature can be inhibited. To ensure the geometric alignment of the pin-fins with the jet flows (at exit), the only means of reducing the flow curvature are thus using additional jets or decreasing the spacing between the pin-fins. The use of flanking jets is seen as necessary for a blockage pin-fin setup.

The pin-fins do not significantly affect the affect the curvature of the jets leading up to impingement. If the pin-fins are sufficiently close to the jet exit, then curvature of the jets may even be considered negligible. Depending on the severity of curvature the flow interacting with the pin-fins is asymmetric about the pin-fin center. Certain regions just upstream of the pin-fin may have a near-zero velocity magnitude. Once the flow impinges on the pin-fin however there is some portion of the flow that is redirected around the outer side of the pin-fin surface. This redirected flow was sufficient to delay the curvature of a flanking jet.

At the end-wall, the flow patterns around a pin-fin subjected to an impinging orifice jet share similarities to those of a pin-fin subjected to an impinging tube jet. The presence of an upstream obstacle, such as the perforated blockage that formed the orifice jets, may distort end-wall flow patterns. If the blockage is sufficiently close, there are increased flows along the blockage surface. The increased flow interacting with the perforated blockage would be beneficial to the cooling performance of a blockage pin-fin setup, requiring the first row of pin-fins to be positioned closer to the blockage surface.

When multiple pin-fins are subjected to impinging orifice jets, the end-wall flows can vary significantly from those around a single pin-fin. This is in contrast to multiple pin-fins subjected to a uniform flow where the end-wall flows still strongly resemble the standard horseshoe vortex structures around a single pin-fin. In a blockage pin-fin setup, the end-wall flows between pin-fins intersect and this results a band of disrupted flow that extends upstream to the blockage. This band of flow entrains the downstream wake flows from the pin-fins preventing their convergence. The band may then result in a flow field interacting with a second pin-fin row that is distinct from that seen by the first row. This process is expected to repeat, with unique end-wall flow patterns at successive rows, until the jet flow has diffused, and a uniform-like flow is established through the array. The lack of convergence also means that a nonstaggered pin-fin array is not recommended for a blockage pin-fin setup.

Thus, an optimal configuration of a blockage pin-fin cooling setup would need to utilize flanking jets, have the pin-fins positioned at the tip of or within the potential core of the jets, and utilize a staggered pin-fin array.

Data Availability Statement

The datasets generated and supporting the findings of this article are obtainable from the corresponding author upon reasonable request.

Nomenclature

D = pin-fin diameter, m
D_j = jet (orifice) diameter, m
H = test channel height, m
l = spacing between downstream surface of perforated blockage and leading-edge of pin-fins, m
l_B = spacing between perforated blockage plates, m
l_p = length of the jet potential core, m
Re_j = Reynolds number based on jet diameter
S_{z1} = spanwise spacing between pin-fin centers, m
S_{z2} = spanwise spacing between jet centers, m
t = thickness of perforated blockage plate, m
U = flow velocity in the streamwise (x) direction, m/s
V = flow velocity in the spanwise (z) direction, m/s
v = flow velocity magnitude, m/s
v_e = jet velocity at exit, m/s
W = test channel width, m
x = an axis coinciding with the streamwise direction of flow and nominal jet axis
y = an axis coinciding with the height of the channel, parallel to the pin-fin axis
z = an axis coinciding with the spanwise direction of flow and perpendicular to the nominal jet axis
μ = dynamic viscosity, N s/m^2
ρ = density, kg/m^3

References

[1] Krause, D. A., Mongillo, D. J., Soechting, F. O., and Zelesky, M. F., 1999, "Turbomachinery Airfoil With Optimised Heat Transfer," U.S. Patent No. 5,931,638.
[2] Kan, R., Ren, J., and Jiang, H., 2014, "Combined Effects of Perforated Blockages and Pin Fins in a Trailing Edge Internal Cooling Duct," ASME Paper No. GT2014-25767.
[3] Kim, Y., Choi, S. M., Park, H. S., Kim, S. W., Jung, E. Y., Park, J. S., and Cho, H. H., 2019, "Heat Transfer Characteristics of the Rib Angle in the Pin-Fin Cooling Combined With Perforated Blockage," Trans. Korean Soc. Mech. Eng. B, **43**(7), pp. 453–461.

Downloaded from http://asmedigitalcollection.asme.org/fluidsengineering/article-pdf/doi/10.1115/1.4064008/7230895/fe_146_05_051302.pdf by The Nanjing University Of Aeronautics & Astronautics user on 18 January 2024

[4] Baker, C. J., 1980, "The Turbulent Horseshoe Vortex," J. Wind Eng. Ind. Aerodyn., **6**(1–2), pp. 9–23.
[5] Schekman, S., Atkins, M. D., and Kim, T., 2019, "Local End-Wall Heat Transfer Enhancement by Jet Impingement on a Short Pin-Fin," Int. J. Heat Mass Transfer, **128**, pp. 1033–1047.
[6] Goldstein, R. J., and Chen, S. B., 1998, "Flow and Mass Transfer Performance in Short Pin-Fin Channels With Different Fin Shapes," Int. J. Rotating Mach., **4**(2), pp. 113–128.
[7] Chyu, M. K., Hsing, Y. C., and Natarajan, V., 1998, "Convective Heat Transfer of Cubic Fin Arrays in a Narrow Channel," ASME J. Turbomach., **120**(2), pp. 362–367.
[8] Ghahremanian, S., Svensson, K., Tummers, M. J., and Moshfegh, B., 2014, "Near-Field Mixing of Jets Issuing From an Array of Round Nozzles," Int. J. Heat Fluid Flow, **47**, pp. 84–100.
[9] Gordon, E. B., and Gerber, I., 1990, "The Entrainment Rate for a Row of Turbulent Jets," NASA, OH, Report No. CR-185278.
[10] Laban, A., Aleyasin, S. S., Tachie, M. F., and Koupriyanov, M., 2019, "Experimental Investigation of Nozzle Spacing Effects on Characteristics of Round Twin Free Jets," ASME J. Fluids Eng., **141**(7), p. 071201.
[11] Svensson, K., Rohdin, P., and Moshfegh, B., 2016, "On the Influence of Array Size and Jet Spacing on Jet Interactions and Confluence in Round Jet Arrays," ASME J. Fluids Eng., **138**(8), p. 081206.
[12] Tanaka, E., 1974, "Interference of Two-Dimensional Parallel Jets–2. Experiments on the Combined Flow of Dual Jet," Bull JSME, **17**(109), pp. 920–927.
[13] Tanaka, E., 1969, "The Interference of Two-Dimensional Parallel Jets: 1st Report Experiments on Dual Jet," Trans. Jpn. Soc. Mech. Eng., **35**(274), pp. 1257–1264.
[14] Gauntner, J. W., Livingood, B., and Hrycak, P., 1970, "Survey of Literature on Flow Characteristics of a Single Turbulent Jet Impinging on a Flat Plate," NASA, Washington, DC, Report No. TN D-5652 NTIS N79-18963.
[15] Hrycak, P., Lee, D. T., Gaunter, J. W., and Livingood, J. N. B., 1970, "Experimental Flow Characteristics of a Single Turbulent Jet Impinging on a Flat Plate," NASA, Washington, DC, Report No. TN D-5690.
[16] Moon, S. W., and Lau, S. C., 2003, "Heat Transfer Between Blockages With Holes in a Rectangular Channel," ASME J. Heat Mass Transfer-Trans. ASME, **125**(4), pp. 587–594.
[17] Shin, S., and Kwak, J. S., 2008, "Effect of Hole Shape on the Heat Transfer in a Rectangular Duct With Perforated Blockage Walls," J. Mech. Sci. Technol., **22**(10), pp. 1945–1951.
[18] Park, J. S., Jo, Y. H., and Kwak, J. S., 2016, "Heat Transfer in a Rectangular Duct With Perforated Blockages and Dimpled Side Walls," Int. J. Heat Mass Transfer, **97**, pp. 224–231.
[19] Ahn, H. S., Lee, S. W., Lau, S. C., and Banerjee, D., 2007, "Mass (Heat) Transfer Downstream of Blockages With Round and Elongated Holes in a Rectangular Channel," ASME J. Heat Mass Transfer-Trans. ASME, **129**(12), pp. 1676–1685.
[20] Lau, S. C., Cervantes, J., Han, J. C., Rudolph, R. J., and Flannery, K., 2003, "Measurements of Wall Heat (Mass) Transfer for Flow Through Blockages With Round and Square Holes in a Wide Rectangular Channel," Int. J. Heat Mass Transfer, **46**(21), pp. 3991–4001.
[21] Wang, X. L., Yan, H. B., Lu, T. J., Song, S. J., and Kim, T., 2014, "Heat Transfer Characteristics of an Inclined Impinging Jet on a Curved Surface in Crossflow," ASME Int. J. Heat Transfer, **136**(8), p. 081702.
[22] Lim, K. B., Lee, C. H., Sung, N. W., and Lee, S. H., 2007, "An Experimental Study on the Characteristics of Heat Transfer on the Turbulent Round Impingement Jet According to the Inclined Angle of Convex Surface Using the Liquid Crystal Transient Method," Exp. Therm. Fluid Sci., **31**(7), pp. 711–719.
[23] Liu, Y. Y., Schekman, S. W., Bhaiyat, T. I., Lu, T. J., and Kim, T., 2022, "Impingement Cooling of an Isoflux Flat Plate by Blockage Jet," Appl. Therm. Eng., **209**(118239), pp. 118239–12.
[24] Ward-Smith, A. J., 1971, *Pressure Losses in Ducted Flow*, Cambridge University Press, London.
[25] Chyu, M. K., 1990, "Heat Transfer and Pressure Drop for Short Pin-Fin Arrays With Pin-Endwall Fillet," ASME J. Heat Mass Transfer-Trans. ASME, **112**(4), pp. 926–932.
[26] McNaughton, K. J., and Sinclair, C. G., 1966, "Submerged Jets in Short Cylindrical Flow Vessels," J. Fluid Mech., **25**(2), pp. 367–375.
[27] Nguepnang, M. A., Boer, M., and Kim, T., 2016, "Stagnation Heat Transfer on a Concave Surface Cooled by Unconfined Slot Jet," J. Thermophys. Heat Trans., **30**(3), pp. 558–566.
[28] Atkins, M. D., and Kim, T., 2015, "Isotropic-Planar Illumination for PIV Experiments," Exp. Fluids, **56**(3), p. 63.
[29] Baker, C. J., 1979, "The Laminar Horseshoe Vortex," J. Fluid Mech., **95**(2), pp. 347–367.
[30] Kim, T., Lu, T. J., and Song, S. J., 2016, *Application of Thermo-Fluidic Measurement Techniques: An Introduction*, Butterworth-Heinemann, Oxford, UK.
[31] Coleman, H. W., and Steele, W. G., 2018, *Experimentation, Validation, and Uncertainty Analysis for Engineers*, Wiley, Hoboken, NJ.
[32] Westerweel, J., 2000, "Theoretical Analysis of the Measurement Precision in Particle Image Velocimetry," Exp. Fluids, **29**(7), pp. S003–S012.
[33] Adrian, R. J., and Westerweel, J., 2011, *Particle Image Velocimetry*, Cambridge University Press, London.
[34] Westerweel, J., 2008, "On Velocity Gradients in PIV Interrogation," Exp. Fluids, **44**(5), pp. 831–842.

Downloaded from http://asmedigitalcollection.asme.org/fluidsengineering/article-pdf/doi/10.1115/1.4064008/7230895/fe_146_05_051302.pdf by The Nanjing University Of Aeronautics & Astronautics user on 18 January 2024